# Kinetics of lamellar formation on sparsely stripped patterns

Nan Xie, Weihua Li, Hongdong Zhang, Feng Qiu, and An-Chang Shi

Citation: The Journal of Chemical Physics **139**, 194903 (2013); doi: 10.1063/1.4830396
View online: http://dx.doi.org/10.1063/1.4830396
View Table of Contents: http://scitation.aip.org/content/aip/journal/jcp/139/19?ver=pdfcov
Published by the AIP Publishing

# Kinetics of lamellar formation on sparsely stripped patterns

Nan Xie,[1] Weihua Li,[1,a)] Hongdong Zhang,[1] Feng Qiu,[1] and An-Chang Shi[2]
[1]*State Key Laboratory of Molecular Engineering of Polymers, Department of Macromolecular Science, Fudan University, Shanghai 200433, China*
[2]*Department of Physics and Astronomy, McMaster University, Hamilton, Ontario L8S 4M1, Canada*

(Received 9 September 2013; accepted 1 November 2013; published online 18 November 2013)

Chemical epitaxy based on the self-assembly of block copolymers is viewed as a promising technique to achieve ordered patterns on a large scale. Herein, we study the kinetics of lamellar formation of block copolymers under the direction of sparsely stripped patterns using cell dynamics simulations of the time-dependent Ginzburg-Landau theory. First, a scaling law is unveiled with the ordering time of lamellae, $t_p$, with respect to the multiples between the periods of lamellae and stripe patterns, which is consistent with the power law evolution of the correlation length existing in the bulk phase of lamellae. Second, the tolerative windows of perfect order, with deviation from integer multiples, are also estimated from the aspect of kinetics. The results of the ordering time and tolerative windows are of great interest for relevant experiments or applications. Finally, a two-stage evolution is explored during the pattern formation of chemical epitaxy by probing into the evolution of defects, which is of fundamental interest for us to understand the coarsening kinetics of block copolymers under the direction of chemical patterns. © *2013 AIP Publishing LLC*. [http://dx.doi.org/10.1063/1.4830396]

## I. INTRODUCTION

Directed-assembly of block copolymers (BCPs) has been viewed as a promising "bottom-up" strategy in nanotechnology due to its ability to generate perfectly ordered nanostructures with feature size of sub-30 nm and with a molecular precision.[1–7] Thin films prepared via this technique have been applied in many fields, including fabrications of microfluidic devices, quantum dots, magnetic storage media, flash memory devices, integration in advanced lithography.[3,8–13] Recently in semiconductor industry, conventional photolithography cannot meet the demands of shrinking scale of devices, whose resolution requirements are already beyond the ability of visible light.[14] It is increasingly complicated and hugely costly to bring the resolution of photolithography to sub-100 nm and below. So directed assembly of BCPs has emerged as a fascinating alternative approach to overcome the resolution limitation in semiconductor industry.[13,15–18]

BCPs are a class of macromolecules composed of chemically distinct blocks. Driven by immiscibility and connectivity between blocks, BCPs separate into microphase and thereby form a rich variety of periodic structures. For diblock copolymer, the simplest BCP, its equilibrium morphologies such as lamella, gyroid, Fddd, hexagonally packed cylinder, and a lattice of body-center-cubic spheres have been not only experimentally screened but also theoretically verified.[19] Importantly, their feature sizes, in a range of 10–100 nm, make them of particular interest for nanomanufacturing. In the typical soft condensed systems of BCPs, however, defects are usually unavoidable because their appearance only results in a penalty of minuscule free energy. Consequently, these emerging defects destroy the long-range order in BCPs formed morphologies, and thus keep BCP self-assembly from practical applications. Pursuing the goal of realizing full potential of BCPs, researchers propose a great many approaches to yield defect-free patterns, such as chemical epitaxy, topographical epitaxy, solvent-assisting annealing, electric fields, thermal gradients, and shear flow.[2,4,17,20–29] These approaches succeed in varied degrees on the road of guiding the self-assembly of BCPs and achieving long-range order in thin films.

Among approaches mentioned above, chemical epitaxy which makes use of selective interactions between patterns on modified substrates and blocks of polymer to direct the assembly of BCPs, was early reported in 1997 by Rockford *et al.*[30] In this pioneering work, the pattern order was enhanced within a very limited extent. Many research groups have focused on the development of this promising technique by precisely designing chemical patterns. The research group of Nealey successfully imparts both long-range translation and orientation order in thin films of hexagonally packed cylindrical and lamellar BCPs respectively.[3,4,31,32] Additionally, non-regular and non-periodic ordered patterns could be fabricated on a large scale of microns utilizing this strategy as well.[4,33] In these preliminary studies, periodic patterns, only one-to-one corresponding to the feature size of BCPs in bulk, are achieved on patterned substrates by Nealey *et al.*[3,4,31,32] These substrates are usually obtained via electron-beam lithography (EBL) due to its ability of producing feature sizes of 15–25 nm. Considering EBL as a serial processing technique, time consumed in preparation of master substrates is undesirably long.[29] It necessitates the introduction of substrates with sparsely chemical patterns in chemical epitaxy. Recently, several groups independently apply this technique in fabrications of thin films with perfectly ordered lamellae or hexagonally packed cylinders under the guidance of sparsely chemical patterns.[34–37] For lamellar patterns, the directing

a)Author to whom correspondence should be addressed. Electronic mail: weihuali@fudan.edu.cn

 

efficiency of substrates in these experiments has been drastically improved, e.g., reaching a multiple of four.[35] Improvement of directing efficiency offers a direct way to the reduction of making cost of substrates, and thus advances BCP chemical epitaxy toward practical applications. Density multiplication (DM), the ratio between domains and substrate patterns, is a convenient quantity to evaluate the directing efficiency of sparsely chemical substrates. Such is it natural that researchers are expecting substrates with sparser chemical patterns for higher efficiency. But the directing ability of substrates will be attenuated when the patterns on substrates are getting sparser, and eventually fails with defects. This gives rise to a limit of DM of effective substrates. The limit of DM provides a useful guide for experiments to adopt an appropriate pattern period during the preparation of substrates. Suffering from the small excess free energy of defects and the concomitant extremely long relaxation time, it is formidable for bulk BCPs to self-assemble into large-scale ordered morphologies. The substrate patterns not only suppress the emergence of defects but also facilitate their annihilation, and therefore accelerate the ordering process of the entire sample. If and only if the ordering time when the entire sample evolves into perfect order, $t_p$, is feasible in real experiments, the implementation of substrate patterns makes sense. Therefore, it is mandatory to carry out systematic explorations on the ordering kinetics of BCP assembly under the direction of chemical patterns.

Not only it should be emphasized from the application's perspective, understanding of coarsening kinetics of BCPs but also attracts enormous attention of theoretical researchers in academia. During past decades, coarsening kinetics of BCPs is yet less understood because of its well complexity. The long-range order often gives way to defects that would maintain the correlation length, $\xi$, within a range of $10–100L_0$ where $L_0$ is the bulk period of morphologies formed by BCPs. Harrison *et al.*[38] and Ruiz *et al.*,[39] respectively, studies the time dependence of the correlation length and conclude that it increases with time as $\xi \sim t^{\eta}$. Although the values of $\eta$ in their studies are different, they are all around 0.25. These results are well consistent with theoretical predictions of Vega *et al.*[40] and Vinals *et al.*[41] The value of $\eta$ is supposed to depend on the strength of phase separation, thermal noise, and specific types of length scales studied.[40] Anyhow, the evolution of correlation length as time obeys a universal power law. As a result of this slow coarsening kinetics, ordered regions rarely extend beyond microns. In typical cases, a long time annealing (e.g., 3–7 days) is required to attain nanostructures with desirable ordering degree via BCPs self-assembly.[3,4,42]

A number of theoretical researchers have dedicated to the study of BCPs assembly directed by chemical patterns. With Monte Carlo (MC) simulation on a lattice model, Wang *et al.* investigate morphologies of lamella-forming BCPs under the direction of surface patterns.[43] Recently, a MC simulation technique based on the coarse-grained model is successfully developed by de Pablo *et al.*, and used to rationalize experimental observations on the morphologies formed by symmetric BCPs confined between two substrates with chemical patterns.[44] Additionally, with this simulation scheme, Nagpal *et al.* study the stabilities of typical defects observed in thin films of lamella-forming BCPs on stripped substrates by experiments from the aspect of thermodynamics.[45] Focusing on the one-to-one directing case, they have investigated the influences of the strength of potential fields and the incommensurability between the BCP lamellae and the substrate stripes on the stability of different defects. Their results suggest that the strength of potential fields plays a critical role on destabilizing the defects, i.e., directing the morphology toward perfect order. In contrast, the self-consistent field theory (SCFT), which is based on the description of continuous configurations, is an alternative approach in the study of BCPs self-assembly. With two-dimensional (2D) SCFT calculations, Petera *et al.* study the formation of lamellar patterns on patterned substrates.[46] It is found that tilt lamellae arise as a compromise while the period of chemical patterns is larger than the bulk one. Besides the formation of lamellar patterns, a number of SCFT studies are carried out to investigate the phase behaviors of cylinders. Complementary to numerical SCFT, simulations of single chain in mean field are performed to examine morphologies formed by asymmetric BCPs and many complex morphologies are explored.[47] These previous theoretical results improve our understanding on the equilibrium phases of BCPs in chemical epitaxy. However, in contrast to most of attention on the formation of diverse morphologies within a few periods, the kinetics of structure formation is still in the infancy stage. Additionally, to guide the state-of-the-art experimental research on the BCPs lithography, aiming to generate defect-free patterns on a large scale, kinetic simulations have to be performed on macroscopic sizes comparable to experimental samples. Accordingly, a high-efficient kinetic method of coarse-grained model is urgently needed for this task. The time-dependent Ginzburg-Landau (TDGL) theory, which is a phenomenological kinetic model and its implementation by cell dynamics simulation (CDS) has been proven to be high efficient, satisfies this demand.[16,48–50] As a successful demonstration, Li *et al.* study defect evolutions in the morphologies of hexagonal cylinders in chemical epitaxy by virtue of TDGL simulations.[51,52] A bottleneck of the directing efficiency, DM $\leq$ 25, is proposed because of the spinodal phase separation. To date, this efficiency limit is not exceeded by relevant experiments.[6] Subsequently, Xie *et al.* develop a new strategy based on heterogeneous nucleations demonstrated by TDGL simulations on diblock copolymer/homopolymer blends, which tremendously improves the directing efficiency, i.e., DM as large as 128.[53] Based on these fruitful achievements, TDGL is speculated as an effective tool for the description of collective kinetics of BCPs, especially for cases where the size-effect and computation-efficiency are of particular importance.

Periodic lamellar domains are one of geometric simple patterns useful for nanofabrication in semiconductor industry.[33] A number of studies, including experiments and simulations, are attracted and focused on manufacturing ordered lamellar patterns by the directed self-assembly of BCPs. However, there still exist several unresolved and attractive issues, including the ordering time (i.e., the annealing time in experiments), the directing efficiency (or the DM bottleneck), and the tolerative resolution in the fabrication of substrate patterns. Aiming to solve above problems of interest, we focus

on the formation kinetics of lamellar patterns of symmetric BCPs under the direction of chemical patterns using high efficient TDGL simulations.

## II. THEORY AND MODEL

A system composed of symmetric BCPs with equal monomer size and the total polymerization $N$, is considered by us. Each polymer chain consists of A and B blocks with equal polymerization, i.e., $N_A = N_B$, which gives the volume fraction $f_K = N_K/N = 0.5$ ($K = A$ or $B$). The kinetics of phase separation in BCPs can be described by the Cahn-Hilliard model, where the difference of local volume fractions $\phi(\mathbf{r}, t) = \phi_A(\mathbf{r}, t) - \phi_B(\mathbf{r}, t)$ is chosen as the order parameter. For this BCP sample of conserved order parameter, the dynamic equation is given as

$$\frac{\partial \phi(\mathbf{r}, t)}{\partial t} = M\nabla^2 \frac{\delta F[\phi(\mathbf{r}, t)]}{\delta \phi(\mathbf{r}, t)} + \xi(\mathbf{r}, t), \tag{1}$$

where $M$ is a phenomenological positive constant and $\frac{1}{V}\int_V d\mathbf{r}\phi(\mathbf{r}, t) = \overline{\phi} = f_A - f_B = 0$. The last term $\xi(\mathbf{r}, t)$ in Eq. (1) is a thermal noise term, satisfying the fluctuation-dissipation theorem:

$$\begin{aligned} \langle \xi(\mathbf{r}, t)\rangle &= 0, \\ \langle \xi(\mathbf{r}, t)\xi(\mathbf{r}', t')\rangle &= -\eta_0 M\nabla^2 \delta(\mathbf{r} - \mathbf{r}')\delta(t - t'), \end{aligned} \tag{2}$$

where $\eta_0$ indicates the magnitude of the thermal noise. The term of free energy in Eq. (1), $F[\phi(\mathbf{r}, t)]$, is composed of three parts, the short-range energy $F_S[\phi(\mathbf{r}, t)]$, the long-range energy $F_L[\phi(\mathbf{r}, t)]$ and external field adsorption energy:

$$F[\phi(\mathbf{r}, t)] = F_S[\phi(\mathbf{r}, t)] + F_L[\phi(\mathbf{r}, t)] + \int d\mathbf{r} H_{\text{ext}}(\mathbf{r})\phi(\mathbf{r}, t). \tag{3}$$

The short-range energy, arises from the local interactions between blocks, is written as type of Ginzburg-Landau energy:

$$F_S[\phi(\mathbf{r}, t)] = \int d\mathbf{r} \left\{ \frac{C}{2}(\nabla\phi(\mathbf{r}, t))^2 + W[\phi(\mathbf{r}, t)] \right\}. \tag{4}$$

Here the constant C is the diffusion coefficient. The second term of RHS, $W[\phi(\mathbf{r}, t)]$, is defined by $dW[\phi(\mathbf{r}, t)]/d\phi = -A\tanh[\phi(\mathbf{r}, t)] + \phi(\mathbf{r}, t)$, where $A$ determines the immiscibility degree between the two species. The long-range energy results from the connectivity of A and B blocks, which alters macroscopic phase separation into microscopic one. In 1986, Ohta and Kawasaki derived an effective functional form of the long-range interaction for diblock copolymers,[54] which is given by a Green function as

$$\begin{aligned} F_L[\phi(\mathbf{r}, t)] &= \frac{\alpha}{2}\int d\mathbf{r}\int d\mathbf{r}' G(\mathbf{r}, \mathbf{r}')\delta\phi(\mathbf{r}, t)\delta\phi(\mathbf{r}', t) \\ -\nabla^2 G(\mathbf{r}, \mathbf{r}') &= \delta(\mathbf{r} - \mathbf{r}'), \end{aligned} \tag{5}$$

where $\delta\phi(\mathbf{r}, t) = \phi(\mathbf{r}, t) - \overline{\phi}$, and the constant $\alpha$ is coherent to the polymerization and the volume fraction. The last term in Eq. (3) is the external field energy acting as the selective interaction of the patterns. A similar potential-well function as our previous work[51] is applied to describe the adsorption of each striped potential well for A-blocks, which is aligned along Y-axis:

$$H_{\text{ext}}(x, y) = -\frac{1}{2}V_0\{\tanh[(-|x - x_i| + \eta)/\lambda] + 1\}, \tag{6}$$

where $x_i$ ($i = 0, 1, \ldots, N_s$) is the position of the $i$th potential well, and while $|x - x_i| \geq 2\eta$, $H_{\text{ext}}(x, y) = 0$. Here, $V_0$, $\eta$, and $\lambda$ quantify the field strength, the width, and the steepness of each potential well, respectively. The integer $N_s$ is the repeating number of striped patterns across the entire sample. Inserting Eqs. (3)–(6) into Eq. (1), we obtain the final evolution equation of morphologies as

$$\begin{aligned} \frac{\partial \phi(\mathbf{r}, t)}{\partial t} &= M\nabla^2\{-C\nabla^2\phi(\mathbf{r}, t) - A\tanh[\phi(\mathbf{r}, t)] \\ &\quad + \phi(\mathbf{r}, t) + H_{\text{ext}}(\mathbf{r})\} \\ &\quad - M\alpha\delta\phi(\mathbf{r}, t) + \xi(\mathbf{r}, t). \end{aligned} \tag{7}$$

For the sake of efficiency, we consider the cases of thin films in 2D simulations, where the small film thickness has negligible impact on the formation of patterns. This simplification enables us to focus on the samples as large as microns. By virtues of CDS simulation, we simulate Eq. (7) on a square lattice and approximate the Laplacian operator into $\langle\langle X\rangle\rangle - X$, which is written as

$$\langle\langle X\rangle\rangle = \frac{1}{6}\sum X_{NN} + \frac{1}{12}\sum X_{NNN}, \tag{8}$$

where $X_{NN}$ or $X_{NNN}$ indicates the nearest neighboring or the next nearest neighboring sites of X. Previous studies show that the average in Eq. (8) optimizes the stability of the CDS equations. Periodic boundary conditions are imposed on each direction. The forward Euler algorithm is utilized for the time integration.

Following our previous work, we set these parameters in Eq. (7) as $M = 1.0$, $A = 1.26$, $\alpha = 0.02$, $\eta = 0.15L_0$, $C = 1.0$, and $\lambda = 0.50$. In general cases of CDS, grid spacings $\delta x$, $\delta y$ and time step $\delta t$ can be set as large as 1. It is convenient to choose the grid spacing as the length unit. Thus, the size of the simulated box is determined by the grid numbers, i.e., $N_x \times N_y$. To accommodate to the stripe patterns, $N_x$ is set as the nearest integer of the expression, $N_s \times L_0 \times n$, where $n$ is the value of DM.

## III. RESULTS AND DISCUSSION

Obviously, the directing effect is heavily dependent on the commensurate degree between the periods of the stripe patterns and the bulk lamellae. Therefore, it is necessary to determine the bulk period $L_0$ in advance. Through Fourier transformation of density profiles in 2D simulations, we obtain $L_0 \approx 7.86$. To ensure the simulated samples large enough, $N_y$ is fixed as 1024, and $N_x$ is kept around 1000 by regulating the value of $N_s$ for different $n$. Consequently, the simulated system contains more than 100 periodic lamellar domains. A typical sample is illustrated by the schematic plot in Fig. 1.

In applications targeting on the formation of ordered patterns on a large scale, the ordering time plays a critical role. Only when $t_p$ is acceptable in practice, the ordered patterns

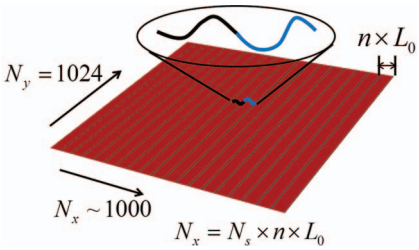


FIG. 1. Schematic plot of directed assembly of BCPs on chemically patterned substrates in 2D. Red color indicates neutral area for two blocks while the blue color indicates the stripes with a preferential interaction to A-block. The stripes are aligned along Y direction.

can be achieved. Otherwise, if the expected ordering time, when all defects are annihilated, is longer than real evolution time $t$, some defects will survive. And the defect concentration is dependent on the deficit of evolution time, $t_p - t$. Accordingly, we focus on exploring the relation between the ordering time and the characteristic of stripe patterns (e.g., DM and commensurate degree) and understanding the ordering mechanism of lamellar patterns in chemical epitaxy via probing into defect evolutions. The knowledge on the ordering time is a useful guide for experiments to set annealing time for specific stripe patterns on the one hand, and the insight on the underlying mechanism is helpful to improve the design of directing patterns on the other hand.

### A. Integer density multiplication

Intuitively, an integer DM is the most favorable for the stripe patterns to direct ordered lamellae. So we first study the kinetics of structure formation of BCPs in these ideal samples with variable integer $n$ between 3 and 16. Here, the field strength is fixed as $V_0 = 0.10$. For each $n$, $t_p$ is calculated by averaging over eight independent runs, each of which is quenched from a disordered state generated by random initial conditions. In each run, whether the morphology reaches its perfect state is checked via detecting the defects, every $10^3$ time steps when $t \leq 10^4$ and otherwise every $10^4$ time steps, using a standard method proposed by Qian and Mazenko (more details will be given in Subsection III C).[55] When no defects are detected in the morphology, the simulation is terminated, and the time $t$ is recorded as $t_p$.

Typical snapshots of density profiles for a given $n = 8$ are presented in Fig. 2. There are a number of notable features. First, ripely separated domains in Fig. 2(a) at $t = 1000$ indicate that the phase separation occurs suddenly as soon as the simulation is triggered from the disordered state because of the spinodal phase separation. Second, well aligned lamellae are formed immediately with precisely registered positions on the stripes after the phase separation. The stronger segregation around the stripes as well as the propagation of aligning order beyond the extent of stripes suggests that the field strength $V_0 = 0.10$ is very high. The preformed ordered lamellae directed by stripe patterns divide the entire sample into $N_s$ identical subsections, each of which becomes uncorrelated and thus evolves independently. The morphology in each subsection is still intervened by a mess of defects which

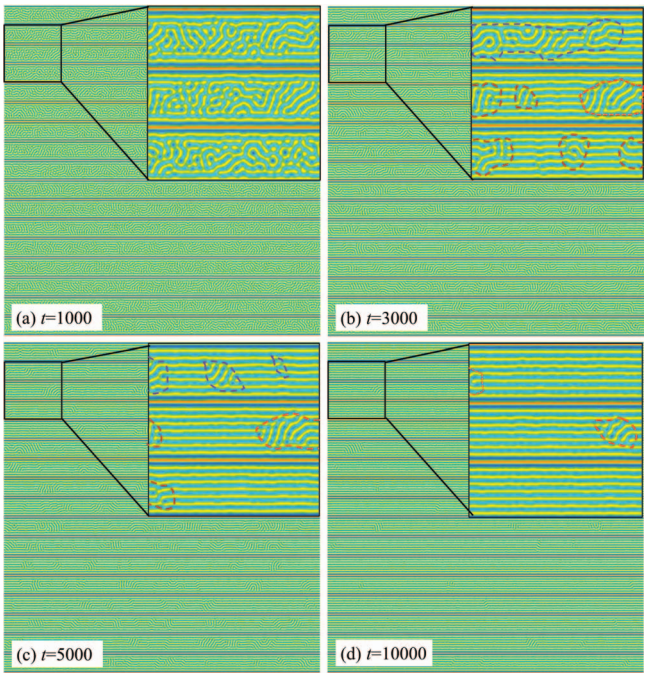


FIG. 2. Typical snapshots of density profiles of A-block with $n = 8$ and $V_0 = 0.10$ at (a) $t = 1000$, (b) $t = 3000$, (c) $t = 5000$, and (d) $t = 10\,000$. The insets are the enlarged portion in the small box for each snapshot, where defect domains are highlighted by dashed lines in different colors.

are not well separated at the initial stage in Fig. 2(a). As time, more and more isolated domains with mismatched orientation from that of stripes are formed, and here these domains are defined as defect domains. The third interesting feature is that some big defect domains (indicated by purple dashed-lines) tend to split into a number of child domains while the others (indicated by red dashed-lines) as well as the new-born child domains directly shrink until evanishing. The splitting behavior is induced by the meeting of the propagation ordering events triggered by two neighboring stripes.

Obviously, the ordering time is dependent on the value of DM, $n$. The ordering time for varying $n$ is determined in our simulations, and that as function of $n$ is drawn into a double-logarithm plot in Fig. 3. This function of ordering time can be well fitted into linear formula except for a few

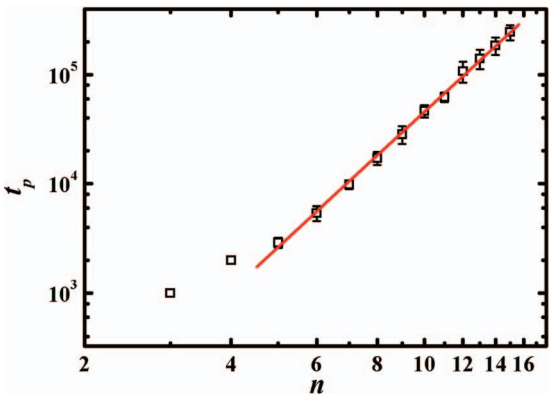


FIG. 3. The ordering time $t_p$ is a function of $n$ in the logarithm-logarithm plot. The solid line is the linear fit of the data.

points at small value of $n$. This linear relation implies that the ordering time is dependent on $n$ with a power law function as $t_p \sim n^{1/\nu}$, where $\nu$ is estimated as 0.25. In the bulk lamellar morphologies, the evolution of correlation length $\xi$ is often used to measure the ordering process. It has been proposed that $\xi$ evolves as time according to the power law of $\xi \sim t^{\eta}$, where $\eta$ is between 0.20 and 0.30. In the current sample, the morphologies become perfectly ordered as soon as the correlation length is comparable to the period of stripes because the entire sample has been divided into independent subsections by these stripes. Consequently, the largest correlation length to be reached during evolution can be seen approximately as $n \times L_0$. By virtue of the bulk formula of correlation length, we get $n \times L_0 \sim t_p^{\eta}$, i.e., $t_p \sim n^{1/\eta}$. This simple analysis directly interprets the nice agreement between the coefficients $\nu$ in the samples of chemical epitaxy and $\eta$ from the bulk systems, and implies that the defects in each subsection obey the similar evolving mechanism as those in bulk. This power law relation clearly shows a scenario how the ordering time depends on DM in the samples with ideal commensurability. In particular, the large coefficient of power law indicates that the expected ordering time is tremendously prolonged for a small increment of $n$. For example, with $n = 8$, the ordering time $t_p = 17\,200$. When $n$ is only increased to 9, $t_p$ goes up to 28 400, which is 65% longer than that of $n = 8$. Note that the deviation of the points at small $n$ simply arises from the time interval used in the check of perfect order which is comparable to the magnitudes of $t_p$ on these points. In other words, the values of $t_p$ are overestimated.

In order to verify the universal power law relation with respect to the field strength, which can be readily modulated by the time and dose of exposure in experiments, a number of magnitudes, $V_0 = 0.050, 0.010, 0.005$, and 0.001, are considered in our simulations. Our results show that perfectly ordered lamellae can be achieved for $n < 16$ with the first three field strengths, but longer ordering time is required for weaker field strength. For example, given $n = 10$, the ordering time $t_p = 46\,500$, 51 400, 92 000, and 504 900 for $V_0 = 0.10, 0.05, 0.01$, and 0.005, respectively. In contrast, for the last systems with $V_0 = 0.001$, the morphologies are still not perfectly ordered even when $t$ exceeds $10^6$, which corresponds to a feasible annealing time in experiments (e.g., 1–3 days). The influence of field strength on the ordering process can be directly manifested by the comparison of density profiles in the early stage, $t = 1000$, for a given $n = 8$ in Fig. 4. Obviously, the ability, that the striped potential wells facilitate the formation of well aligned lamellae which guide the ordering evolution of other portions of morphology, is weakened by the reduction of field strength. In other words, more and more defects cross over the field stripes, and thus make these subsections become less and less independent. In particular, for $V_0 = 0.001$, the existence of stripe patterns is indiscernible in the morphology, and as a consequence, the ordering process is similar as that in the bulk. Apparently, a critical value of $V_0$ for ordered morphologies is between 0.001 and 0.005, and $V_0 \approx 0.05$ is an ideal value because it gives a fairly similar directing effect as that of higher $V_0 = 0.10$. A universal power law is verified in the samples of $V_0 = 0.05, 0.01, 0.005$ with slightly different coefficients within a narrow range of

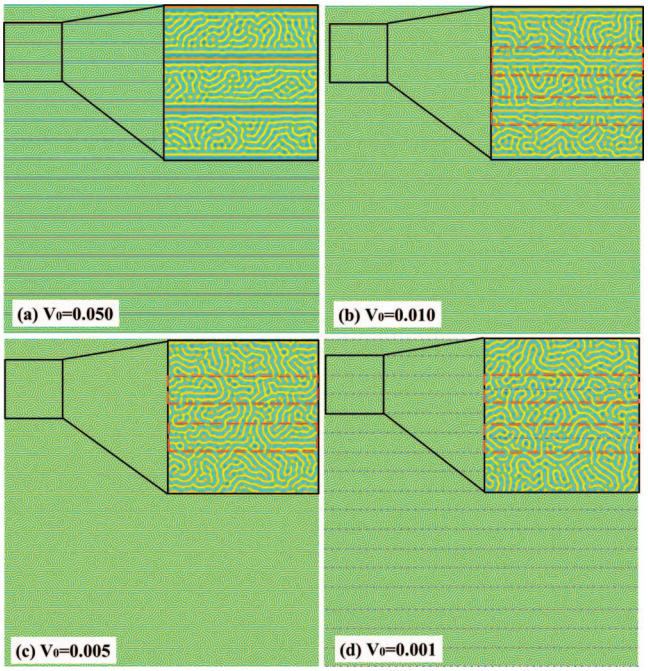


FIG. 4. Typical snapshots of density profiles at $t = 1000$ with $n = 8$ for different $V_0$. The insets are the enlarged portion in the small box for each snapshot, where the area of chemical patterns and vicinity are highlighted by red dashed-line box in (b), (c), and (d). Purple dotted-lines are imposed in (d) to indicate the indiscernible locations of stripe patterns.

$0.25 \sim 0.30$. Our kinetic results are in good agreement with those of thermodynamics by Nagpal *et al.* which suggest that the stability of defects is sensitive to the field strength.[45] In the view of kinetics, defects with higher stability survive for a longer time.

### B. Non-integer density multiplication

During the achievement of ordered nanostructures via directed assembly of BCPs, substrates with periodic chemical patterns play a central role in the whole ordering process. During the fabrication of stripe patterns via the electron beam or extreme ultraviolet lithography technique, an error is inevitably introduced into the value of DM and makes it deviate from ideal integer multiples. This incommensurability induced by the small deviation will result in more packing frustration of domains between the BCP period and the stripe period, and thereby impact the ordering process of morphologies. Accordingly, we systematically investigate the dependence of ordering time on the degree of incommensurability. The ordering time of varying $n$, between 2.3 and 7.5 with an increment of 0.1, for fixed $V_0 = 0.10$ is shown in Fig. 5(a), and accordingly, a window for perfectly ordered patterns is determined by setting a time cutoff as $10^6$ in Fig. 5(b). Intuitively, the landscape of free energy of BCPs is always corrugated by the packing frustration arising from the incommensurability. In kinetics, the evolution of samples with non-integer $n$ are more easily trapped in a metastable state than those with integer $n$. Consequently, a longer ordering time is needed for the samples with higher degree of incommensurability. For example, the ordering time is 10 000, 14 200,

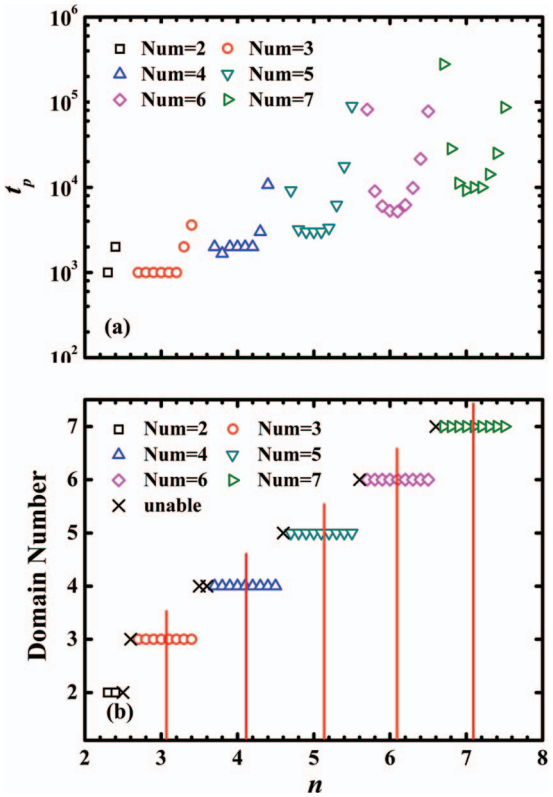


FIG. 5. (a) Ordering time $t_p$ as a function of varying $n$. (b) Domain number (Num) plot of lamellae formed on the substrates with varying $n$, where red lines indicate the estimated centers of windows of perfectly ordered lamellae, $n_0$. Open symbols indicate ordered patterns while crosses indicate unordered ones within a time cutoff, $10^6$.

11 200, and 279 000 for $n = 7.1$, 7.3, 6.9, and 6.7 while the ordering time of $n = 7.0$ is 9200. These results give a definite emphasis on the resolution control in the fabrication of substrates on the one hand, and suggest that a certain degree of incommensurability can be tolerated by the systems on the other hand but at expense of longer ordering time. So long as the expected ordering time is feasible in practical experiments, the ordered lamellar pattern can be generated. Note that the center of windows in Fig. 5(b), indicated as $n_0$, is slightly larger than the corresponding integer $n$. It suggests that BCP domains prefer to be stretched when suffering the incommensurability of periods, which is consistent with the results of Nagpal *et al.*[45] Centering around $n_0$, the logarithm of ordering time, $\ln(t_p)$, can be approximated as a quadratic function of $(n - n_0)$, i.e., $\ln(t_p) \sim (n - n_0)^2 + \ln(t_{p,0})$, where $t_{p,0}$ is the ordering time of corresponding $n_0$. Ross *et al.* proposed that the free energy deviation induced by the incommensurability can be estimated as $\delta E \sim (n - n_0)^2$.[7] As a consequence, we get $t_p \sim e^{\delta E}$, which is similar as the well-known kinetic Arrhenius equation.

### C. Defect evolution during the ordering process

To understand the ordering mechanism of BCP lamellar patterns under the direction of sparsely striped patterns, it is necessary for us to probe into the evolution of defects during the ordering process. Here, we adopt the method proposed by Qian and Mazenko[55] to identify defects, which is illustrated in Fig. 6 of both the bulk sample and directed sample. First, the density configuration with or without potential fields in Fig. 6(a) or 6(d) is transformed into scalar fields in Fig. 6(b) or 6(e), which quantify the local orientation in a range of $(-90^\circ, 90^\circ]$. Compared with the bulk sample, there exists a predominant orientation with lamellae in the directed sample, which is guided by the stripe patterns. In addition, these domains, defined as defect domains with mismatched orientations from the predominant one, are isolated islands in the sea of ordered domains. Usually, defects are clustered on the boundaries of these domains. And then, the finite differential method is applied onto the scalar fields to identify these defects as in Figs. 6(c) and 6(f). In order to quantify the defect evolution, defect concentration, $\phi_{def}$, is introduced and defined as the ratio of defect area (e.g., the red dots in Figs. 6(c) and 6(f)) to the entire sample area. For the directed samples, the number of defect domains, $N_{dm}$, is also recorded as a complementary quantity for revealing the underlying mechanism.

In order to focus on the defect evolution and give prominence to the influence of the DM on it, we choose integer $n$ and fix the field strength $V_0 = 0.10$. The defect concentrations as function of time for $n = 6, 7, \ldots, 16$ are presented in Fig. 7, where that in the bulk is also shown as a comparison (solid line). In bulk samples, the defect concentration, which is conjugated with the correlation length, evolves according to the power-law function discussed before. Obviously, the potential fields alter the evolution of defect concentration into two stages of power law, where the second one has larger coefficient than the first one. In other words, the defect annihilation is accelerated in the second stage, and thus the perfectly ordered pattern can be yielded in a limited time. Therefore, the time, when the morphology evolution enters from the first stage into the second, is critical. We notice that defects go through distinctive evolving behaviors in above two stages: splitting and evanishing via shrinking of defect domains (see Fig. 2). In fact, the two evolving behaviors happen concomitantly while one of them is dominant in a specific stage. The number of defect domains, $N_{dm}$, which is a relevant quantity to clarify the dominant behavior, is determined and given in Fig. 8(a). There is a marked maximal number of defect domains during the evolution, which divides the defect evolution into splitting and evanishing dominant stages. In the first stage, splitting large defect domains into a number of subdomains dominates over evanishing of small domains, thereby increasing $N_{dm}$. After the maximum point, the decrease of $N_{dm}$ indicates that evanishing becomes dominant instead in the second stage. Interestingly, the critical time $t_{max}$ as a function of $n$ in Fig. 8(b) has a similar power law behavior as the ordering time $t_p$.

After entering the second stage, defect domains evolve independently and shrink until evanishing. These defect domains in samples with distinct $n$ assemble similar characteristics except for their sizes which are determined by the period of stripe patterns. In kinetics, they share the similar evolving behavior. This feature can be directly illustrated by the evolution of defect concentration with a time shift of corresponding $t_{max}$ in Fig. 9. That the second-stage portions of these curves for diverse $n$ are well

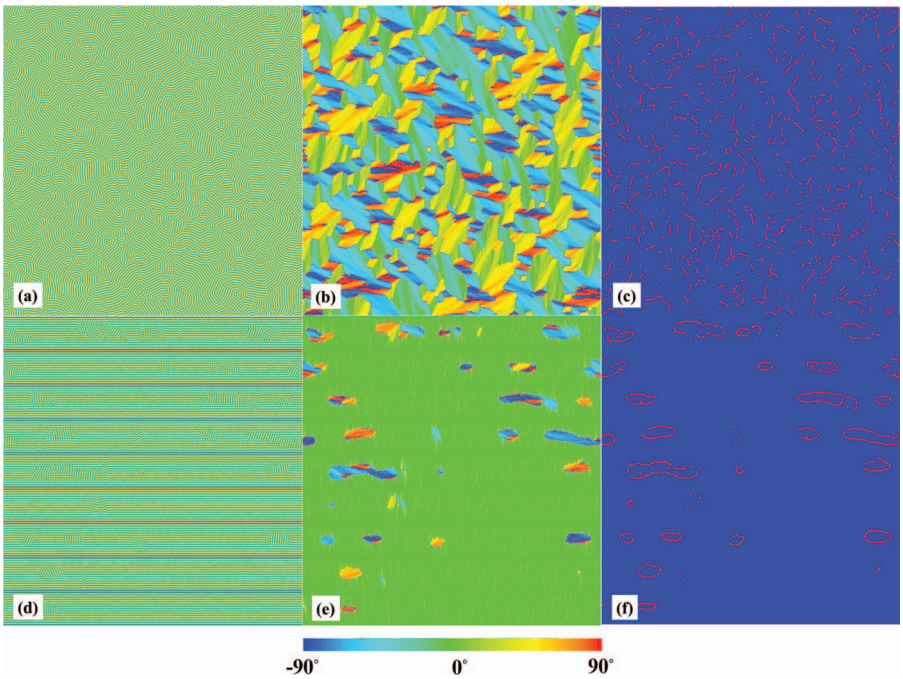


FIG. 6. Illustration of identifying defects in the sample with (bottom row) or without (upper row) stripe patterns. The figures in three columns from left to right correspond to density configurations [(a) and (d)], scalar fields of orientation [(b) and (e)], and defect distributions [(c) and (f)] (defects are plotted into red color), respectively. The color spectrum indicates local orientation of lamellar domains in a range of $(-90^\circ, 90^\circ]$.

overlapped justifies that the common evolution is a typical power law.

During the directing processes of BCP self-assembly, ordered patterns are often achieved by imposing an anisotropic force, such as electrical field, shearing flow, and thermal gradient. In the present directing scheme of chemical epitaxy, the anisotropy is introduced by the stripe patterns. In contrast, this anisotropic property is localized near the stripes, which affords the two-stage ordering evolution discussed above. As an example, we focus on the sample, $n = 15$ and $V_0 = 0.10$, to examine the appearance of anisotropy during ordering processes. Here $l_x$ and $l_y$ are used to characterize the average sizes of defect domains along X- and Y-axis, respectively. In Fig. 10, both $l_x$ and $l_y$ decline to zero when all defect domains shrink toward evanishing. Obviously, the presence of anisotropy originating from the stripe patterns results in different declining speed between $l_x$ and $l_y$. For $l_y$, in the first stage of evolution, the dominant splitting events induce a sharp drop from an initial value which is comparable with the size of entire sample along Y-axis. In contrast, $l_x$ with an

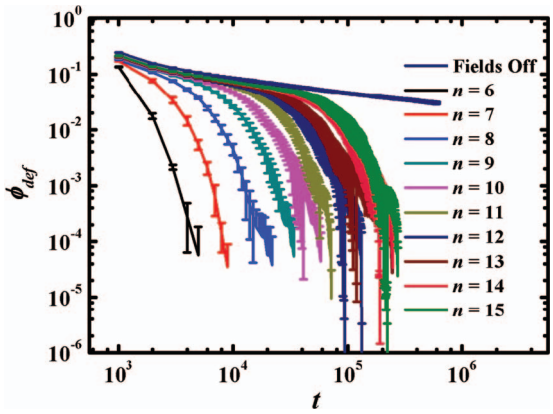


FIG. 7. Evolution of defect concentrations for various $n$ in a logarithm-logarithm plot. As a comparison, the data in the bulk are indicated by the solid line.

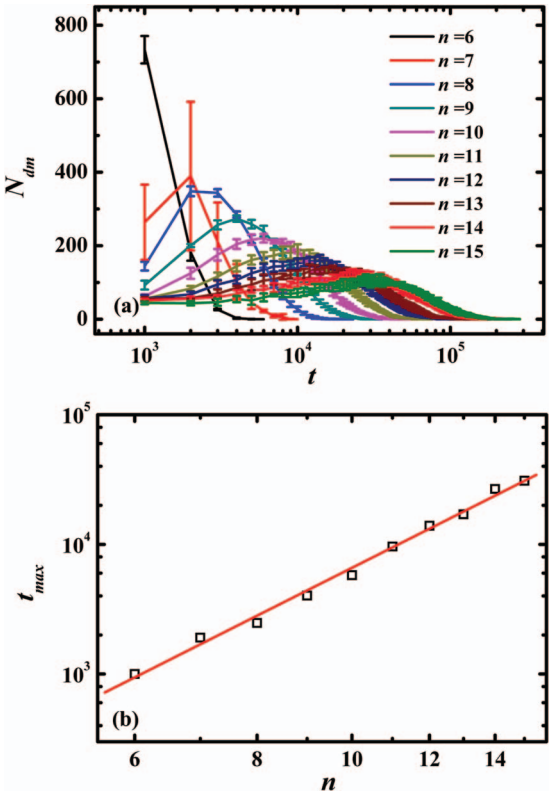


FIG. 8. (a) Evolution of the number of defect domains, $N_{dm}$, for $n = 2, 3, \ldots, 16$, and $V_0 = 0.10$. (b) critical time $t_{max}$ with respect to $n$. The red line is the linear fit to the data.

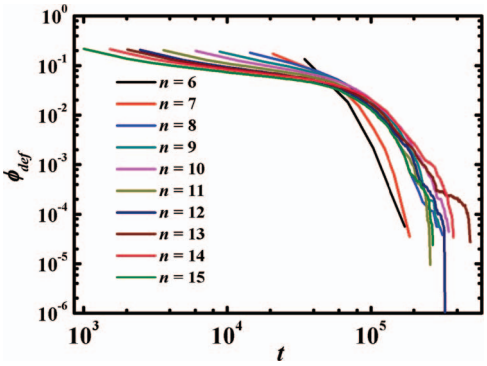


FIG. 9. The defect concentration curves of Fig. 7 are shifted with corresponding critical time $t_{max}$. For the reason of clarity, the error bars are not shown.

initial value comparable with $n \times L_0$ decreases slowly. This provides a further support for the existence of splitting events.

### D. Conclusions

In summary, we study in a systematic manner the evolution of lamellae formed by symmetric BCPs under the direction of sparsely stripe patterns. Our results unveil a scaling law between the ordering time and integer density multiplication, which is proven to arise from the power law found in the bulk. Importantly, this scaling law is universal with $V_0$ as long as $V_0$ is strong enough for the direction of ordered patterns. With samples of non-integer density multiplication, the impact of the degree of incommensurability on the ordering time is investigated and well described by an Arrhenius-like kinetic formula. This indicates that the incommensurability in a certain degree can be kinetically tolerated in the directing scheme at the expense of prolonging annealing time. Our results provide a useful guide for the estimation of expected ordering time with a given integer or non-integer density multiplication. In addition, to understand the underlying ordering mechanism in depth, we probe into the evolution of defects. A two-stage evolution, splitting dominant and evanishing dominant, is proposed. In the first stage, large defect domains tend to split into subdomains and thus the number of defect domains is increased. Whereas, in the second stage, most of defect domains shrink until evanishing, which leads to a continuous decrease in the number of defect domains. Furthermore, the role of anisotropy arising from the stripe patterns on the ordering evolution is also discussed via tracing the average sizes, $l_x$ and $l_y$, of defect domains as time. Based on the above results, the directing stripes take effect on the ordering evolution of lamellae in two aspects. On the one hand, the periodic stripes divide the large sample into narrow subsections in x direction, thereby speeding up the ordering evolution along X-axis. On the other hand, the ordering of lamellae propagates from the locations of stripes where well registered lamellae are preformed at the initial stage, and it penetrates the subsections, which divides large defect domains into subdomains along Y-axis. Therefore, the reduced size along Y-axis accelerates the shrinking process of these defect domains further.

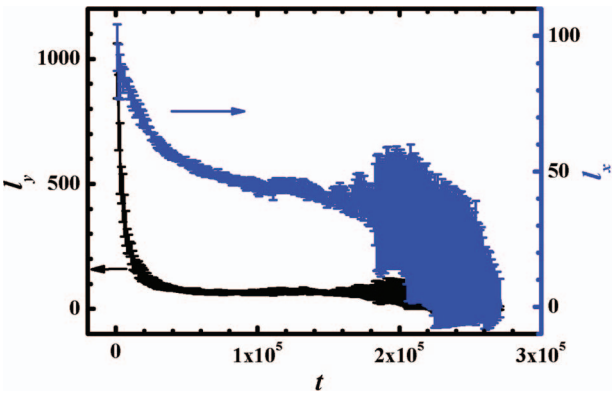


FIG. 10. Evolution of the average sizes of defect domains along X/Y-axis, $l_x$ and $l_y$.

Although our simulations are performed in 2D, where our model corresponds to perpendicular lamellar morphology formed in a thin film without considering the effect of film thickness, our results of the ordering time and the ordering mechanism are commonly useful for perpendicular lamella-forming thin films in experiments. In the case of chemical epitaxy, as a limited strength of fields can be usually generated by surface chemical modification, a high DM cannot be achieved.[35] In fact, our model with a strong field is particularly suitable to describe the perpendicular lamellar formation under the direction of geometrical trenches which has been realized in experiments, where a higher DM has been yielded.[56,57] In addition, our results are instructive for the formation of parallel cylinders formed in trenches because of the similar smectic ordering process. We can expect a similar scaling law with the ordering time but with a different coefficient.

## ACKNOWLEDGMENTS

This work was supported by the National Natural Science Foundation of China (NNSFC) (Grant Nos. 21322407 and 21174031).

[1]K. W. Guarini, C. T. Black, Y. Zhang, I. V. Babich, E. M. Sikorski, L. M. Gignac, 2003 IEEE International Electron Devices Meeting, Technical Digest (IEEE, Washington, DC, 2003), pp. 541.
[2]M. Park, C. Harrison, P. M. Chaikin, R. A. Register, and D. H. Adamson, Science **276**, 1401 (1997).
[3]S. O. Kim, H. H. Solak, M. P. Stoykovich, N. J. Ferrier, J. J. de Pablo, and P. F. Nealey, Nature (London) **424**, 411 (2003).
[4]M. P. Stoykovich, M. Müller, S. O. Kim, H. H. Solak, E. W. Edwards, J. J. de Pablo, and P. F. Nealey, Science **308**, 1442 (2005).
[5]R. A. Segalman, H. Yokoyama, and E. J. Kramer, Adv. Mater. **13**, 1152 (2001).
[6]I. Bita, J. Yang, Y. S. Jung, C. A. Ross, E. L. Thomas, and K. K. Berggren, Science **321**, 939 (2008).
[7]J. Y. Cheng, A. M. Mayes, and C. A. Ross, Nature Mater. **3**, 823 (2003).
[8]D. C. Duffy, J. C. McDonald, and O. J. A. Schueller, Anal. Chem. **70**, 4974 (1998).
[9]Q. L. Zhang, T. Xu, D. Butterfield, M. J. Misner, D. Y. Ryu, T. Emrick, and T. P. Russell, Nano Lett. **5**, 357 (2005).
[10]R. F. Service, Science **314**, 1868 (2006).
[11]L. W. Chang, T. L. Lee, C. H. Wann, C. Y. Chang, H.-S. P. Wong, 2009 IEEE International Electron Devices Meeting (IEEE, 2009), pp. 821.
[12]C. T. Black, R. Ruiz, and G. Breyta, IBM J. Res. Dev. **51**, 605 (2007).
[13]C. J. Hawker and T. P. Russell, TP MRS Bull. **30**, 952 (2005).

[14]ITRS International Technology Roadmap for Semiconductors. 2010 Updates and 2009 Chap. Lithography. See http://www.itrs.net/Links/2010ITRS/Home2010.htm.
[15]C. Park, J. Yoon, and E. L. Thomas, Polymer **44**, 6725 (2003).
[16]I. W. Hamley, Angew. Chem., Int. Ed. **42**, 1692 (2003).
[17]R. A. Segalman, Mater. Sci. Eng. R. **48**, 191 (2005).
[18]M. P. Stoykovich and P. F. Nealey, Mater. Today **9**, 20 (2006).
[19]F. S. Bates and G. H. Fredrickson, Annu. Rev. Phys. Chem. **41**, 525 (1993); M. W. Matsen and M. Schick, Phys. Rev. Lett. **72**, 2660 (1994); C. A. Tyler and D. C. Morse, *ibid.* **94**, 208302 (2005).
[20]D. E. Angelescu, J. H. Waller, D. H. Adamson, P. Deshpande, S. Y. Chou, R. A. Registe, and P. M. Chaikin, Adv. Mater. **16**, 1736 (2004).
[21]C. T. Black, K. W. Guarini, K. R. Milkove, S. M. Bakers, T. P. Russell, and M. T. Tuominen, Appl. Phys. Lett. **79**, 409 (2001).
[22]J. Y. Cheng, R. A. Ross, E. L. Thomas, H. I. Smith, and G. J. Vansco, Appl. Phys. Lett. **81**, 3657 (2002).
[23]S. H. Kim, M. J. Misner, and T. P. Russell, Adv. Mater. **16**, 2119 (2004).
[24]T. L. Morkved, M. Lu, A. M. Urbas, E. E. Ehrichs, H. M. Jaeger, P. Mansky, and T. P. Russell, Science **273**, 931 (1996).
[25]P. Mansky, Y. Liu, E. Huang, T. P. Russell, and C. Hawker, Science **275**, 1458 (1997).
[26]T. Thurm-Albrecht, J. Scotter, G. A. Kastle, N. Emley, T. Shibauchi, L. Krusin-Elbaum, K. Guarini, C. T. Black, M. T. Tuominen, and T. P. Russell, Science **290**, 2126 (2000).
[27]T. Hashimoto, J. Bodycomb, Y. Funaki, and K. Kimishima, Macromolecules **32**, 952 (1999).
[28]B. C. Berry, A. W. Bosse, J. F. Douglas, R. L. Jones, and A. Karim, Nano Lett. **7**, 2789 (2007).
[29]A. P. Marencic and R. A. Register, Annu. Rev. Chem. Biomol. Eng. **1**, 277 (2010).
[30]L. Rockford, Y. Liu, P. Mansky, T. P. Russell, M. Yoon, and S. G. J. Mochrie, Phys. Rev. Lett. **82**, 2602 (1999).
[31]E. W. Edwards, M. P. Stoykovich, H. H. Solak, and P. F. Nealey, Macromolecules **39**, 3598 (2006).
[32]A. M. Welander, H. M. Kang, K. O. Suen, H. H. Solak, M. Müller, J. J. de Pablo, and P. F. Nealey, Macromolecules **41**, 2759 (2008).
[33]M. P. Stoykovich, H. M. Kang, P. F. Nealey, K. C. Daoulas, G. L. Liu, C. C. Liu, J. J. de Pablo, M. Müller, and P. F. Nealey, ACS Nano **1**, 168 (2007).
[34]R. Ruiz, H. Kang, F. A. Detcheverry, E. Dobisz, D. S. Kercher, T. R. Albrecht, J. J. de Pablo, and P. F. Nealey, Science **321**, 936 (2008).
[35]J. Y. Cheng, C. T. Rettner, D. P. Sanders, H. C. Kim, and W. D. Hinsberg, Adv. Mater. **20**, 3155 (2008).
[36]Y. Tada, S. Akasaka, H. Yoshida, H. Hasegawa, E. Dobisz, D. Kercher, and M. Takenaka, Macromolecules **41**, 9267 (2008).
[37]Y. Tada, S. Akasaka, M. Takenaka, H. Yoshida, R. Ruiz, E. Dobisz, and H. Hasegawa, Polymer **50**, 4250 (2009).
[38]C. Harrison, D. H. Adamson, Z. D. Cheng, J. M. Sebastian, S. Sethuraman, D. A. Huse, R. A. Register, and P. M. Chaikin, Science **290**, 1558 (2000); C. Harrison, Z. D. Cheng, S. Sethuraman, D. A. Huse, P. M. Chaikin, D. A. Vega, J. M. Sebastian, R. A. Register, and D. H. Adamson, Phys. Rev. E **66**, 011706 (2002).
[39]R. Ruiz, R. L. Sandstrom, and C. T. Black, Adv. Mater. **19**, 587 (2007).
[40]D. A. Vega, C. Harrison, D. E. Angelescu, M. L. Trawick, D. A. Huse, P. M. Chaikin, and R. A. Register, Phys. Rev. E **71**, 061803 (2005).
[41]J. Vinals, J. Phys. Soc. Jpn. **78**, 041011 (2009).
[42]F. A. Detcheverry, P. F. Nealey, and J. J. de Pablo, Macromolecules **43**, 6495 (2010).
[43]Q. Wang, Q. Yan, P. F. Nealey, and J. J. de Pablo, Macromolecules **33**, 4512 (2000).
[44]F. A. Detcheverry, G. L. Liu, P. F. Nealey, and J. J. de Pablo, Macromolecules **43**, 3446 (2010).
[45]U. Nagpal, M. Mueller, P. F. Nealey, and J. J. de Pablo, ACS Macro. Lett. **1**, 418 (2012).
[46]D. Petera and M. Muthukumar, J. Chem. Phys. **109**, 5101 (1998).
[47]K. C. Daoulas, M. Muller, M. P. Stoykovich, H. Kang, J. J. de Pablo, and P. F. Nealey, Langmuir **24**, 1284 (2008).
[48]I. W. Hamley, Macromol. Theory Simul. **9**, 363 (2000).
[49]Y. Oono and S. Puri, Phys. Rev. Lett. **58**, 836 (1987); Phys. Rev. A **38**, 434 (1988); S. Puri and Y. Oono, *ibid.* **38**, 1542 (1988).
[50]M. Pinna and A. V. Zvelindovsky, Eur. Phys. J. B **85**, 210 (2012).
[51]W. H. Li, F. Qiu, Y. L. Yang, and A. C. Shi, Macromolecules **43**, 1644 (2010).
[52]W. H. Li, N. Xie, F. Qiu, Y. L. Yang, and A. C. Shi, J. Chem. Phys. **134**, 144901 (2011).
[53]N. Xie, W. H. Li, F. Qiu, and A. C. Shi, Soft Matter **9**, 536 (2013).
[54]T. Ohta and K. Kawasaki, Macromolecules **19**, 2612 (1986).
[55]H. Qian and G. F. Mazenko, Phys. Rev. E **67**, 036102 (2003).
[56]Y. S. Jung and C. A. Ross, Nano Lett. **7**, 2046 (2007).
[57]S. M. Park, M. P. Stoykovich, R. Ruiz, Y. Zhang, C. T. Black, and P. F. Nealey, Adv. Mater. **19**, 607 (2007).